Complexity Analysis and u-net Based Segmentation of Meningeal Lymphatic Vessels

Nazia Tabassum, Michael Ferguson, Jasmin Herz, and Scott T. Acton

2020 54th Asilomar Conference on Signals, Systems, and Computers | 978-0-7381-3126-9/20/$31.00 ©2020 IEEE | DOI: 10.1109/IEEECONF51394.2020.9443412

***Abstract*—This paper showcases a u-net based architecture for the automated segmentation images of meningeal lymphatic vessels. These lymphatic vessels surround the cerebral cortex and have been recently found to drain waste from the brain. Studies on mice have shown loss of memory and impairment in cognitive ability if the vessels' draining capacity does not function adequately. As the meningeal lymphatic vasculature itself is a recent discovery, there is no software tailored for automatically segmenting these images. Instead, segmentation must be performed by hand, which is a tedious and error-prone process. By building an automatic segmentation tool for these vessels, we can provide informatics for understanding and researching them, in a quick and reliable way. A convolutional neural network, called u-net, is adapted to the vessel segmentation application, with the goal of teaching the network how to segment the vessels. Segmentation using u-net is compared to traditional non-learning based segmentation methods using Dice coefficient. Three complexity measures are also proposed to evaluate the segmentation quality: vessel ramification index, porosity, and vessel length. The existence of a technique and associated software to automatically segment and analyze these vessels will drastically speed up subsequent neuroscience research in the field.**

***Index Terms*—u-net, segmentation, lymphatics, learning, vasculature, complexity, porosity, ramification**

I. Introduction

In recent years, the lymphatic system present in our central nervous system has come to the research forefront. The lymphatic vessels surrounding the brain, which were unknown just six years ago, have been shown to drain waste from our brains. If this waste is not drained, it accumulates to form plaque, which leads to neurodegenerative disease. Studies on mice have shown loss of memory and impairment in cognitive ability in cases where the vessels do not drain waste adequately. [2]

Since these vessels were only recently discovered, there is no tool available for automatically analyzing these images. By building the first such tools, we can provide informatics that enable the understanding these vessels.

The first step in analysis is segmentation, or detection of vessel objects in an image. Neuroscientists currently analyze these image data by hand, laboriously marking the boundaries of vessels. The time required to segment one image into background and foreground regions is around two hours. Manual processing is an incredibly slow and fallible method, and serves as the main hindrance to further research involving this data. The proposed work hopes to alleviate the time taken to process the meningeal lymphatic vessel (MLV) images, and therefore speed up research in the areas using these images.

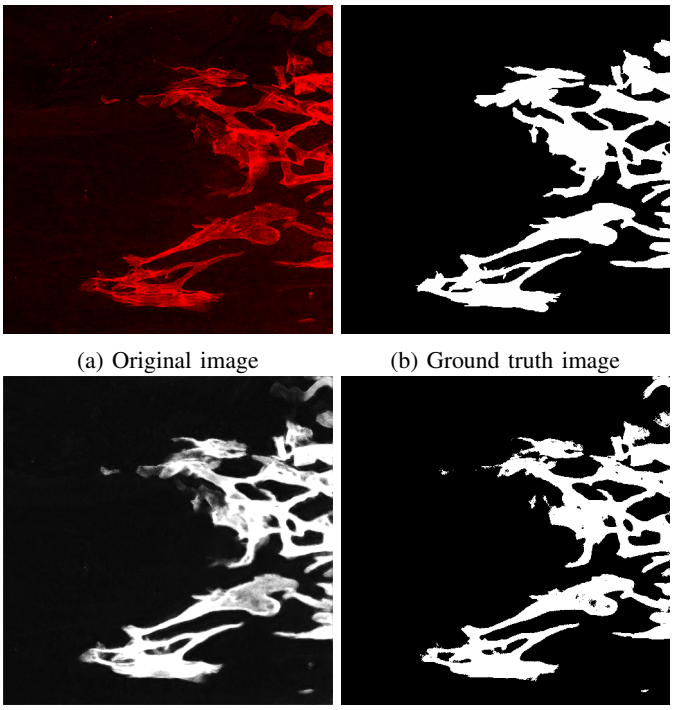

(a) Original image (b) Ground truth image

(c) Confidence map (d) Binary segmentation result

Fig. 1: Example result. The original red channel image (cropped to size 512x512 pixels) is shown in (a), the hand created ground truth in (b). U-net generated confidence map is shown in (c), and the binary segmentation result in (d) is produced by thresholding the confidence map at 50%. The Dice coefficient for this image is 0.89.

Examples of traditional segmentation methods for vascular datasets (neurons, blood vessels, etc.) include level-set segmentation methods [1], [7], [8] and image matting [3]. These methods are proven to work well on vascular data, but in the case of retinal images, deep learning has recently shown promise. Among the most prominent methods of computer vision and machine learning are convolutional neural networks, or CNNs. This paper explores the application of CNNs to segmenting meningeal lymphatic vessels in the brain via

This work is funded by a Double Hoo Grant awarded by the Office of Undergraduate Research at the University of Virginia.

N. Tabassum and S.T. Acton are with the Department of Electrical Engineering, University of Virginia, Charlottesville, VA, 22903 USA. M. Ferguson is with the Department of Computer Science, University of Virginia. J. Herz is with the Department of Pathology and Immunology, Washington University School of Medicine in St Louis, MO, USA. e-mail: {nt5rc, mef8dd, acton}@virginia.edu.

microscopy images, by applying existing medical-based CNN architecture to improve the time taken to process MLV images. An example result from our work is shown in Fig. 1.

Images of MLVs are similar to fundus images in morphology, so using deep learning for segmentation may further enhance the quality of segmentation results. The main challenge with using learning in this area is that the available datasets are not large enough to train networks. For this reason, we choose u-net [10] as the network of choice, because a necessary data augmentation step is built-in to the network pipeline. U-net was designed to handle datasets with few training images. This paper documents the first time application of deep learning to images of this kind.

Neuroscientists also currently process the vessels to quantify certain parameters, such as average width of vessels. This quantification process is also incredibly time consuming, and any measurements would be more accurate and more repeatable if automated. A wider choice of informatics would also yield more information about lymphatic vessels.

Our research questions thus are: can we improve the speed and accuracy of segmenting the meningeal lymphatic vessels by using CNNs as compared to traditional segmentation methods? Also, can complexity measures be tuned specifically for lymphatic vasculature in order to assess and analyze segmentation results?

II. Segmentation

A. Choice of Network

We chose the u-net architecture due to its proven success in biomedical segmentation problems, especially for retinal vessel images [13]. U-net also has built-in methods to augment data, such as rotation, cropping, adding noise/blur, etc. These augmentation techniques are useful for our dataset, as the size is limited.

B. Training Data

One of the central problems of biomedical images in regards to machine learning is the size of the data set; most images are hard to come by because each image represents one (expensive) mouse being sacrificed. The original images of meningeal lymphatic vessels are 2D confocal microscopy image acquired by the Kipnis lab in the University of Virginia department of Neuroscience. There are 39 images in total, which does not constitute a sufficient dataset to train a deep neural network.

Once the data had been processed and augmented, training was ready to begin. The version of u-net we modeled can be found in the following repository [13]. A 3-operator majority voted ground truth was created by the authors and used for training labels. We executed our deformation pipeline and generated 1000 images of size 512x512 to act as training and testing for the ground truth masks and original images, and split those up into 750 training and 249 testing, based off of the original 39 images split into 30 train/9 test. Splitting of the data into train and test datasets occurred prior to data augmentation, making sure not to include any original images or deformed images from training within the test data set. The network then read in and trained on the 750 image pairs, and then was tested on the 249 test images. Data normalization was added after each convolutional layer to further reduce the noise of output images. The network hyperparameters were as follows, as well as the training times and hardware:

1) Training Time: 2 Hours
2) Hardware: Nvidia Titan X and Nvidia Titan XP x2
3) Optimizer: ADAM with $\alpha = 1 * 10^{-5}$ learning rate
4) Loss: Binary Cross Entropy
5) Implemented On: Tensorflow with Keras
6) Number of Epochs: 100
7) Steps/Epoch: 10

In the experiments, the original images varied in size from 4000x2000 to 2000x10000, and the network was only trained on sizes 512x512. This subsampling was performed to aid computation speed. Results are promising with the above configuration on 512x512 size images, as demonstrated below. However, increasing the image size to 1024x1024 created output of an all-black confidence map, which leads us to believe that this method of data augmentation does not generate enough new features for larger image size, possibly leading to vanishing gradients within the CNN [9].

III. Assessing Segmentation Results

The trained u-net was tested on 249 test images, augmented from the real dataset. The u-net output is a confidence map in grayscale, higher confidence represented by higher intensity (on a scale of 0 to 1.) 100 percent confidence that a pixel belongs to the foreground set is denoted by intensity 1, and the color white. Thresholding was performed on the outputted confidence map at 0.5, or 50 percent confidence, to produce a binary segmentation. The confidence maps and binary results are shown in Fig. 1.

Fig. 2 contains images with segmentation results. The original red channel image of meningeal lymphatics is shown in the top left corner. The majority voted ground truth is shown on the top right. The u-net output is a confidence map, which we threshold at confidence level 0.5 to get a binary segmentation result, with resulting Dice coefficient of 0.89. This is a high segmentation result, as the highest value the Dice coefficient can take is 1, which indicates a perfect match with the ground truth. Dice coefficients above 0.8 show strong segmentation performance.

TABLE I: Dice and Hausdorff Distance for Test Set

Metric	Dice Coefficient	Hausdorff Distance (microns)
Average	**0.72**	5.87
Standard Deviation	0.15	1.16
Mode	0.78	4.8
Median	0.76	5.86

This binary segmentation was evaluated compared to the hand-labeled ground truth by using Dice coefficient [12]. A higher Dice coefficient indicates closer alignment with the ground truth. The Hausdorff distance is shown in microns [4],

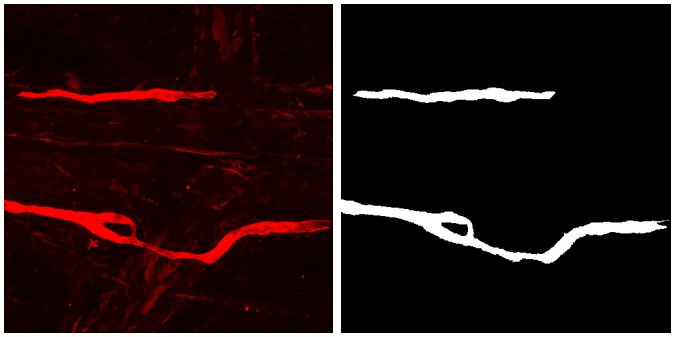

(a) Original image (b) Ground truth image

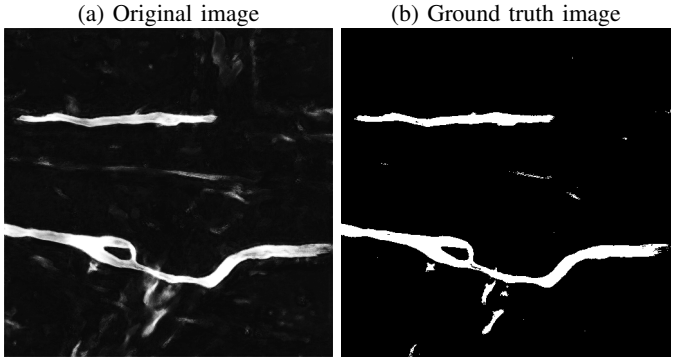

(c) Confidence map (d) Binary segmentation result

Fig. 2: Example result on the partial mount dataset. The original red channel image (cropped to size 512x512 pixels) is shown in (a), the hand created ground truth in (b). U-net generated confidence map is shown in (c), and the binary segmentation result in (d) is produced by thresholding the confidence map at 50%. The Dice coefficient for this image is 0.89.

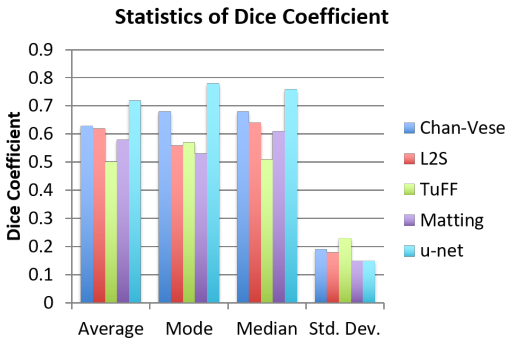

Fig. 3: Statistics of Dice coefficient calculated for all segmentation results.

TABLE II: Dice Coeff. and Hausdorff Dist. (microns) for Competing Methods

Method	**Chan-Vese**		**L2S**		**Mat.**		**TuFF**	
Metric	*Dice*	*Hau.*	*Dice*	*Hau.*	*Dice*	*Hau.*	*Dice*	*Hau.*
Avg.	**0.63**	7.07	**0.62**	6.99	**0.58**	6.98	**0.50**	8.07
Std. Dev.	0.19	1.86	0.18	1.77	0.15	1.59	0.23	2.16
Mode	0.68	6.09	0.56	5.19	0.53	5.09	0.57	6.70
Median	0.68	6.64	0.64	6.86	0.61	7.02	0.51	7.63

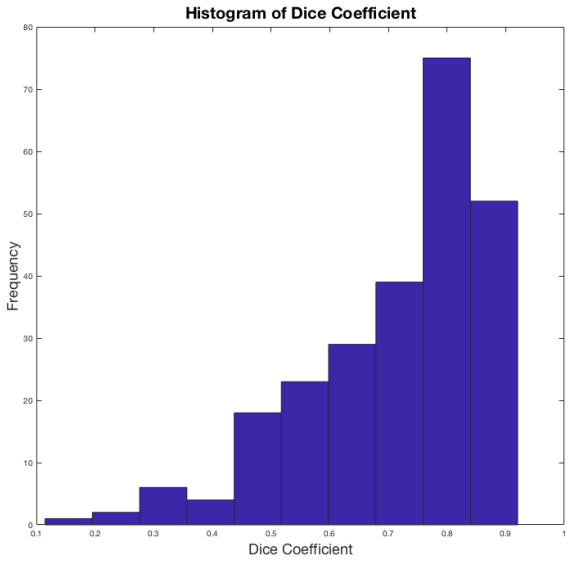

Fig. 4: Histogram of Dice coefficients for test data.

also in Table I. Lower Hausdorff distance means a better match with the ground truth.

The same 249 images were used to test four separate methods for vessel segmentation: Chan-Vese [1], L2S (Legendre Level Set) [7], Hierarchical Image Matting [3], and TuFF (Tubularity Flow Field) [8]. The Dice coefficent was computed for all the results, reading across the top row (in bold), with statistics reported in the subsequent rows. The average Dice coefficient for the segmentation results is 0.72, as shown in Fig. 3. It is clear to see that the average Dice score for u-net, is much higher than any of the competing algorithms, and that the standard deviation is also comparable or lower. Hausdorff distance for the other methods is shown in Table II as well, and it is clear to see that using the other methods produces higher Hausdorff distance than when using u-net for segmentation.

The average Dice coefficent for the segmentation results is 0.72, as shown in Fig. 3. It is clear to see that the average Dice score for u-net, is much higher than any of the competing algorithms, and that the standard deviation is also comparable or lower. Though the average Dice coefficient using u-net is 0.72, in Fig. 4, it is seen that the most frequent Dice coefficient values are between 0.8 and 0.9, which are reasonably high scores in terms of segmentation accuracy.

In Fig. 5 we show results on a spinal lymphatic image with

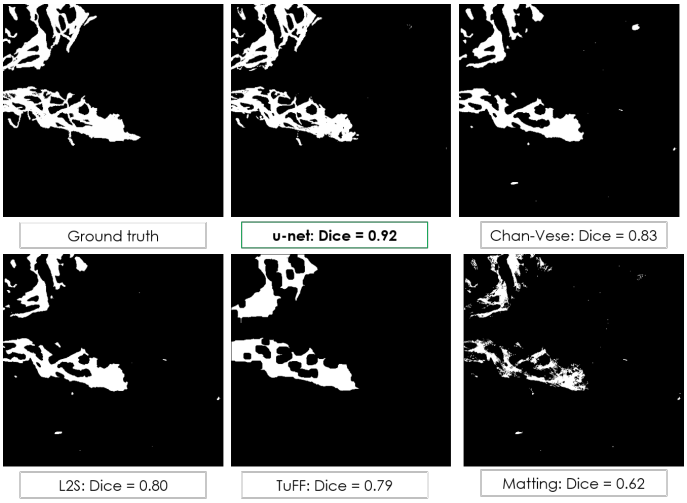

Fig. 5: Example result on the spinal dataset. The original ground truth image (cropped to size 512x512 pixels) is shown in the first panel, the segmentation results following. U-net generated binary segmentation result in the top row is produced by thresholding the confidence map at 50%. The Dice coefficient for this image is 0.92.

other state of the art segmentation methods. Chan-Vese, L2S, and TuFF are all level-set segmentation methods. Hierarchical image matting, in the bottom right corner, is a correlation based segmentation method developed for segmentation of retinal images. Using u-net provides a Dice score of 0.92, a very high Dice score in its own right, and much higher than all the other competing methods. The details in the u-net segmentation result are much clearer, even though the staining in the original image is weak between branches of the vessel.

A. New Measures for Complexity Analysis

To further assess the segmentation results, we introduce three informatics into the study of lymphatic vasculature: vessel length, vessel ramification index, and vessel porosity.

We can first build a skeleton from the segmentation to start the automated complexity analysis. Skeletons are one-pixel wide backbones of image objects. One measure of interest for lymphatic vessels is vessel length. This can measure lymphatic regression; regression is where the vessel grows shorter in length over time, with age. The vessel length is calculated as the total number of pixels along the skeleton, as the skeleton is one-pixel wide. Vessel length was computed for all binary segmentation output by first skeletonizing. This complexity measure is commonly used for neruonal analysis [11].

Another measure of interest is the ramification index. A ramification index has been calculated for cells such as microglia and is typically defined as the ratio of the perimeter of the cell to the area, normalized by the same ratio for a circle of that area. This index quantifies how ramified a cell is, or how spread out the branches (processes) of the microglia are. [6] This index does not directly translate to lymphatic vessels, as the vessels are not a single cell with processes.

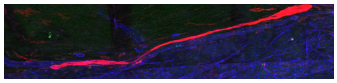

(a) Simple Vessel

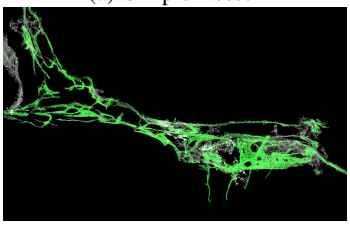

(b) Complex Vessel

Fig. 6: Two types of vessels.

TABLE III: Ramification Indices

Vessel Type	RI	Vessel RI
Simple Vessel	7.50	2.99
Complex Vessel	31.28	21.56

Calculation of the ramification index was performed next on two types of vessels: one simpler vessel, and a "more ramified" vessel. These are both shown in Figure 6. The RI does indeed scale with complexity within vessels. However, there could be more meaningful ways of calculating complexity that are more directly applicable to lymphatic vessels.

A modified ramification measure is proposed here to better fit lymphatic vessels. The approach is to compare the perimeter/area ratio of a vessel to the ratio of a "similar" vessel that has no holes or capillary loops. Instead of comparing to a circle of the same area, the comparison was performed with a simpler, filled vessel - a vessel with one smooth contour all along the outside, a filled vessel. The boundary was traced roughly in Fiji to create a smooth vessel approximation, for visual purposes only. A depiction of the process is shown in Figure 7. As it was done by hand, the boundary is much wider than the vessel (boundary in yellow.) In the experiments, the vessel boundary lies directly on the edge of the vessel.

The vessel ramification index is defined as

$$RI_{new} = \frac{Peri_1}{Area_1} \div \frac{Peri_2}{Area_2}, \tag{1}$$

where $Peri_1$ and $Area_1$ refer to the perimeter and area of the original vessel, and $Peri_2$ and $Area_2$ are the perimeter and area of the simplified vessel. This scales with the original ramification index, with a larger ramification index indicating a more ramified, or complex vessel.

The new RI is able to discriminate distinctively between simpler and more complex vessels. The simpler vessel has a ramification index (RI) of 7.50 and the more complex vessel has an RI of 31.28, with a new RI of 2.99 and 21.56, respectively. These results are depicted in Table III. While the previous RI for microglia also is discriminative between two vessel types, we suggest that the new one developed is more intuitive and informative for the application.

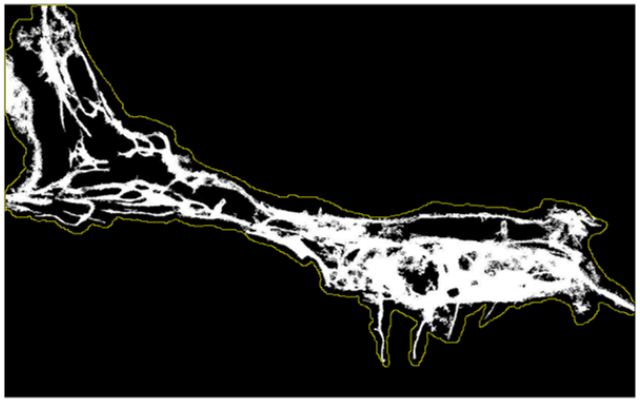

(a) Tracing Vessel Boundary

(b) Simplified Vessel Result

Fig. 7: Simplification of vessel.

Another similar measure we developed is inspired by porosity for materials. Porosity, or void fraction, is a measure of the void or empty spaces in a material. It is the fraction of the volume of voids over the total volume. Porosity is always a number between 0 and 1, unless it is described as a percentage. A material has high porosity if it contains large spaces.

The vessel porosity is calculated as the area of capillary loops, which are the gaps where a vessel branches and reconnects to the larger network, over the total surface area of the vessel. This calculation is similar to the calculation of porosity for materials. We use area instead of volume because the images are 2D. Vessel porosity is similar to ramification index in that it measures how much space is filled within the larger vessel boundary.

TABLE IV: Mean Squared Error of Complexity Measures

Metric	Chan-Vese	L2S	TuFF	Matting	u-net
Length	$3.77\text{x}10^6$	$4.05\text{x}10^6$	$4.24\text{x}10^6$	$2.41\text{x}10^7$	$1.63\text{x}10^6$
RI	0.508	0.515	0.538	0.478	0.228
Porosity	0.015	0.015	0.015	0.015	0.009

All three metrics were run on all segmentation results, and compared to the ground truth using mean squared error. The u-net segmentation results have the lowest error for all three measures compared to the ground truth complexity values, as shown in Table IV.

IV. Conclusion

The main outcome revolves around the improved processing times for the data given. Neuroscientists using the tool need not waste valuable resources on hand quantifying the images. Another glaring issue is that of accuracy and reproducibility; different observers can and do segment the images differently. Therefore, a lack of consistency among the data analysis is prevalent. The complexity measures proposed in this paper are automatically calculated, and would serve to benefit the scientists that wish to use the data to draw conclusions.

Our adaptation of CNNs to the segmentation problem for vessels is also useful for anyone in the future wishing to segment vessel data. Our trained network can be used quickly and efficiently on any new images. Scientists using our tools can spend more time developing a better understanding of the lymphatic system's relationship with disease. There is hope that the onset of disease could be predicted by studying lymphatic vasculature [5]. If so, drugs can be developed (indeed neuroscientists have already started such studies) to improve vessel function and to possibly improve outcomes in diseases such as Alzheimer's.

References

[1] Tony F Chan and Luminita A Vese. Active contours without edges. *IEEE Transactions on image processing*, 10(2):266–277, 2001.

[2] Sandro Da Mesquita, Antoine Louveau, Andrea Vaccari, Igor Smirnov, R Chase Cornelison, Kathryn M Kingsmore, Christian Contarino, Suna Onengut-Gumuscu, Emily Farber, Daniel Raper, et al. Functional aspects of meningeal lymphatics in ageing and alzheimer's disease. *Nature*, 560(7717):185, 2018.

[3] Zhun Fan, Jiewei Lu, Caimin Wei, Han Huang, Xinye Cai, and Xinjian Chen. A hierarchical image matting model for blood vessel segmentation in fundus images. *IEEE Transactions on Image Processing*, 28(5):2367–2377, 2019.

[4] Daniel P Huttenlocher, Gregory A Klanderman, and William J Rucklidge. Comparing images using the hausdorff distance. *IEEE Transactions on pattern analysis and machine intelligence*, 15(9):850–863, 1993.

[5] Antoine Louveau, Tajie H Harris, and Jonathan Kipnis. Revisiting the mechanisms of cns immune privilege. *Trends in immunology*, 36(10):569–577, 2015.

[6] C. Madry, V. Kyrargyri, I.L. Arancibia-Cárcamo, R. Jolivet, S. Kohsaka, R.M. Bryan, and D. Attwell. Microglial ramification, surveillance, and Interleukin-1β release are regulated by the two-pore domain K^+ channel THIK-1. *Neuron*, 97:299–312.e6, jan 2018.

[7] S. Mukherjee and S.T. Acton. Region based segmentation in presence of intensity inhomogeneity using legendre polynomials. *IEEE Signal Proc. Lett.*, 22:298–302, 2015.

[8] Suvadip Mukherjee, Barry Condron, and Scott T Acton. Tubularity flow field–A technique for automatic neuron segmentation. *IEEE Trans. on Image Proc.*, 24(1):374–389, 2015.

[9] Razvan Pascanu, Tomas Mikolov, and Yoshua Bengio. On the difficulty of training recurrent neural networks. In *International conference on machine learning*, pages 1310–1318, 2013.

[10] Olaf Ronneberger, Philipp Fischer, and Thomas Brox. U-net: Convolutional networks for biomedical image segmentation. In *International Conference on Medical image computing and computer-assisted intervention*, pages 234–241. Springer, 2015.

[11] M. Rubinov and O. Sporns. Complex network measures of brain connectivity: Uses and interpretations. *NeuroImage*, 52:1059–1069, 2010.

[12] Thorvald Sørensen. A method of establishing groups of equal amplitude in plant sociology based on similarity of species and its application to analyses of the vegetation on danish commons. *Biol. Skr.*, 5:1–34, 1948.

[13] zhixuhao. unet for image segmentation, 2019.